



## Reversible Control of Hydrogenation of a Single Molecule

Satoshi Katano, *et al.*  
*Science* **316**, 1883 (2007);  
DOI: 10.1126/science.1141410

**The following resources related to this article are available online at [www.sciencemag.org](http://www.sciencemag.org) (this information is current as of July 11, 2007):**

**Updated information and services**, including high-resolution figures, can be found in the online version of this article at:

<http://www.sciencemag.org/cgi/content/full/316/5833/1883>

**Supporting Online Material** can be found at:

<http://www.sciencemag.org/cgi/content/full/316/5833/1883/DC1>

This article **cites 20 articles**, 2 of which can be accessed for free:

<http://www.sciencemag.org/cgi/content/full/316/5833/1883#otherarticles>

This article appears in the following **subject collections**:

Chemistry

<http://www.sciencemag.org/cgi/collection/chemistry>

Information about obtaining **reprints** of this article or about obtaining **permission to reproduce this article** in whole or in part can be found at:

<http://www.sciencemag.org/about/permissions.dtl>

alloy with geophysically relevant Ni concentrations (10 to 15%) should be more stable than the hcp phase, not only at the experimental conditions of this work but also at Earth's core conditions.

The experimentally determined lattice parameter of the bcc Fe<sub>0.9</sub>Ni<sub>0.1</sub> phase at 225 (±10) GPa and 3400 (±100) K is 2.4884 (±2) Å, which corresponds to a molar volume of 4.64 cm<sup>3</sup>/mol and a density of 12.12 g/cm<sup>3</sup>. Under the same conditions, hcp Fe has about 2% higher density (5). The absolute values of the pressure and changes of density depend on the pressure scale adopted and the hcp Fe TEOs (25). If we apply the pressure scale and the hcp Fe TEOs proposed by Dewaele *et al.* (28), the pressure in our experiments could be estimated as 195 GPa. This means that in the absence of accurate and self-consistent TEOs for phases of Fe and Fe-Ni alloys at multimegabar pressure ranges and high temperatures, discussions of the influence of the changes of density produced by the hcp-to-bcc transition of Fe<sub>0.9</sub>Ni<sub>0.1</sub> on the density of Earth's inner core are too preliminary. However, it is clear even at this point that bcc Fe<sub>0.9</sub>Ni<sub>0.1</sub> is less dense than pure hcp Fe, and the budget of the light elements in the inner core could be reduced because of this phase transition. If conservative estimates are made (1, 5), matching of Earth's inner core density to the preliminary reference Earth model (PREM) does not require any light elements, but at the other extreme [low-temperature (~5200 K) estimates at inner/outer core boundary and pure Fe compressibility described by Dewaele *et al.* (28)] the density excess is still about 5%.

The synthesis of bcc Fe<sub>0.9</sub>Ni<sub>0.1</sub> at pressures above 230 GPa and temperatures above 3400 K could have implications for understanding the properties and dynamics not only of Earth's solid inner core but of the liquid outer core as well. Changes in the structure of liquids above subsolidus phase boundaries are well known. If changes from "close-packed-like" to "bcc-like" structures occur in molten Fe-Ni alloy at pressures above 200 GPa, this may affect the density and rheology of Earth's outer core as well as the partitioning of light elements between differently structured parts of the molten core.

#### References and Notes

- H. K. Mao, Y. Wu, L. C. Chen, J. F. Shu, A. P. Jephcoat, *J. Geophys. Res.* **95**, 21737 (1990).
- C. S. Yoo, J. Akella, A. J. Campbell, H. K. Mao, R. J. Hemley, *Science* **270**, 1473 (1995).
- R. Boehler, *Nature* **363**, 534 (1993).
- D. Andrault, G. Fiquet, M. Kunz, F. Viscoekas, D. Häusermann, *Science* **278**, 831 (1997).
- L. S. Dubrovinsky, S. K. Saxena, F. Tutti, T. Le Bihan, *Phys. Rev. Lett.* **84**, 1720 (2000).
- A. B. Belonoshko, R. Ahuja, B. Johansson, *Nature* **424**, 1032 (2003).
- L. Vocadlo *et al.*, *Nature* **424**, 536 (2003).
- D. Anderson, *Theory of Earth* (Blackwell Scientific, Oxford, 1989).
- W. F. Bottke, D. Nesvorný, R. E. Grimm, A. Morbidelli, D. P. O'Brien, *Nature* **439**, 821 (2006).
- J.-F. Lin *et al.*, *Geophys. Res. Lett.* **29**, 109 (2003).
- J.-F. Lin, D. L. Heinz, A. J. Campbell, J. M. Devine, G. Shen, *Science* **295**, 313 (2002).
- L. S. Dubrovinsky *et al.*, *Phys. Rev. Lett.* **86**, 4851 (2001).
- W. L. Mao, A. J. Campbell, D. L. Heinz, G. Shen, *Phys. Earth Planet. Interiors* **155**, 146 (2006).
- E. Huang, W. Basset, M. S. Weathers, *J. Geophys. Res.* **97**, 4497 (1992).
- L. Dubrovinsky, N. Dubrovinskaja, in *High-Pressure Crystallography, NATO Science Series II, Mathematics,*

*Physics and Chemistry*, A. Katrusiak, P. McMillan, Eds. (Kluwer Academic, Dordrecht, Netherlands, 2004), pp. 393–410.

- G. Shen, V. B. Prakapenka, M. L. Rivers, S. R. Sutton, *Phys. Res. Lett.* **92**, 185701 (2004).
- K. C. Creager, *Nature* **356**, 309 (1992).
- X. D. Song, P. G. Richards, *Nature* **382**, 221 (1996).
- W. Su, A. M. Dziewonski, R. Jeanloz, *Science* **274**, 1883 (1996).
- J. E. Vidale, D. A. Dodge, P. S. Earle, *Nature* **405**, 445 (2000).
- P. Ramdohr, *Fortschr. Mineral.* **53**, 165 (1976).
- N. Dubrovinskaja *et al.*, *Phys. Rev. Lett.* **95**, 245502 (2005).
- G. Shen, V. B. Prakapenka, P. J. Eng, M. L. Rives, S. R. Sutton, *J. Synchrotron Radiat.* **12**, 642 (2005).
- P. Loubeyre, F. Occelli, R. LeTouillec, *Nature* **416**, 613 (2002).
- Materials and methods are available as supporting material on Science Online.
- J. M. Brown, R. G. McQueen, *J. Geophys. Res.* **91**, 7485 (1986).
- J. M. Brown, *Geophys. Res. Lett.* **28**, 4339 (2001).
- A. Dewaele *et al.*, *Phys. Rev. Lett.* **97**, 215504 (2006).
- The authors acknowledge financial support by the European Mineral Sciences Initiative (EuroMinSci) of the European Science Foundation, Deutsche Forschungsgemeinschaft, Swedish Research Council, Carl Tryggers Foundation for Scientific Research, Swedish Foundation for Strategic Research, and Hungarian Scientific Research Fund. Help in sample preparation by A. Audéat and S. Dubrovinsky is highly appreciated. Part of this work was performed at GeoSoilEnviroCARS (Sector 13). GeoSoilEnviroCARS is supported by NSF, the U.S. Department of Energy–Geosciences, and the State of Illinois.

#### Supporting Online Material

www.sciencemag.org/cgi/content/full/316/5833/1880/DC1  
Materials and Methods  
Figs. S1 to S4  
References

5 March 2007; accepted 1 May 2007  
10.1126/science.1142105

## Reversible Control of Hydrogenation of a Single Molecule

Satoshi Katano,<sup>1</sup> Yousoo Kim,<sup>1\*</sup> Masafumi Hori,<sup>1,2</sup> Michael Trenary,<sup>3</sup> Maki Kawai<sup>1,2\*</sup>

Low-temperature scanning tunneling microscopy was used to selectively break the N-H bond of a methylaminocarbyne (CNHCH<sub>3</sub>) molecule on a Pt(111) surface at 4.7 kelvin, leaving the C-H bonds intact, to form an adsorbed methylisocyanide molecule (CNCH<sub>3</sub>). The methylisocyanide product was identified through comparison of its vibrational spectrum with that of directly adsorbed methylisocyanide as measured with inelastic electron tunneling spectroscopy. The CNHCH<sub>3</sub> could be regenerated in situ by exposure to hydrogen at room temperature. The combination of tip-induced dehydrogenation with thermodynamically driven hydrogenation allows a completely reversible chemical cycle to be established at the single-molecule level in this system. By tailoring the pulse conditions, irreversible dissociation entailing cleavage of both the C-H and N-H bonds can also be demonstrated.

The scanning tunneling microscope (STM) can be used to induce a variety of processes of individual molecules, including hopping from one site to another, rotations, conformational changes, bond dissociation, and even bond formation reactions (1–4). A particularly powerful way to better understand such molecular manipulations with the STM (5) is to focus on systems that have already been well charac-

terized by conventional surface science methods and to use inelastic electron tunneling spectroscopy (STM-IETS) (6) for chemical identification of reactants and products (1, 7, 8). The latter method provides a vibrational spectrum of individual molecules, and although several recent examples of its use have been reported, the fundamentals of vibrational excitation with tunneling electrons are still an active area of research

(2, 3, 9). We show here that we can selectively break the N-H bond of a single methylaminocarbyne (CNHCH<sub>3</sub>, or CNHMe) molecule, without disturbing the C-H bonds, to produce methylisocyanide (CNCH<sub>3</sub>, or CNMe), and we also can restore the N-H bond at will through an ordinary catalytic hydrogenation reaction. The combination of tip-induced chemistry with surface catalysis thus allows us to produce a repeatable chemical cycle at the single-molecule level.

An earlier study of CNMe on a Pt(111) surface (10) was motivated by a desire to determine whether the well-known modes of bonding of CO to Pt(111) (11) could be extended to a molecule with the isocyanide (-NC) functionality, which is isoelectronic with CO. In the case of CO, the molecule occupies an on-top site at low surface coverages, but at higher coverages oc-

<sup>1</sup>Surface Chemistry Laboratory, RIKEN, 2-1 Hirosawa, Wako, Saitama 351-0198, Japan. <sup>2</sup>Department of Advanced Materials, University of Tokyo, 5-1-5 Kashiwanoha, Kashiwa, Chiba 277-8651, Japan. <sup>3</sup>Department of Chemistry, University of Illinois at Chicago, 845 West Taylor Street, Chicago, IL 60607-7061, USA.

\*To whom correspondence should be addressed. E-mail: maki@riken.jp (M.K.); ykim@riken.jp (Y.K.)

occupies both on-top and twofold bridge sites. More recently, Kang and Trenary (12, 13) showed that CNMe on Pt(111) can be readily hydrogenated to form the methylaminocarbyne species CNHMe. Reflection absorption infrared spectroscopy revealed a large red shift in the N-C stretching frequency, indicative of the rehybridization of the N-C and C-Pt bonds. These previous studies indicated that the reaction changes the adsorption site from on-top for CNMe to a twofold bridge site for CNHMe.

We recently confirmed through observation of individual molecules with the STM (14) that CNMe occupies on-top sites at low coverages and both on-top and twofold bridge sites at higher coverages. In addition to being of fundamental interest, the use of isocyanide derivatives in molecular electronics has attracted attention because of the favorable electrical contact associated with the NC-metal bond (15, 16). In this context, reactions that dramatically alter the hybridization and hence the bond order of the NC group, such as conversion to an aminocarbyne, are of great interest.

All experiments were performed in an ultrahigh-vacuum chamber (base pressure  $3 \times 10^{-11}$  Torr) with a low-temperature STM (LT-STM, Omicron) that had an electrochemically etched tungsten tip. CNMe was synthesized by the method described by Casanova *et al.* (17). The purity of the synthesized CNMe was >99% as checked by a gas chromatograph mass spectrometer. The Pt(111) surface was cleaned by conventional methods described elsewhere (13, 14) and consisted of repeated cycles of  $\text{Ar}^+$  sputtering, annealing to 1100 K, and oxygen exposures at 800 K until a clean atomically resolved Pt(111) surface was observed with the STM. All STM images presented here were obtained with a sample bias of 100 mV, a tunneling current of 1.0 nA, and a substrate temperature of 4.7 K.

An STM image obtained after exposing the clean Pt(111) surface to CNMe at 50 K (Fig. 1A) revealed single CNMe molecules adsorbed at on-top sites as bright protrusions (14). The STM image in Fig. 1B was obtained at 4.7 K after exposure of the CNMe/Pt(111) surface to 1 Langmuir ( $1 \times 10^{-6}$  Torr  $\cdot$ ) of hydrogen ( $\text{H}_2$ ) at 300 K, which Kang and Trenary (12, 13) showed leads to N-protonation of CNMe to CNHMe. Although the general appearance of the STM image was the same before and after hydrogen exposure, the apparent height of the protrusions was reduced from 0.106 nm (CNMe) to 0.085 nm (CNHMe) (Fig. 1C). This apparent height difference of 0.021 nm between the protrusions before and after hydrogen exposure is readily apparent in the line profile shown in Fig. 1C that was taken from the dashed line in Fig. 1D, which was obtained after the surface imaged in Fig. 1B was exposed to additional CNMe at 50 K. The H atoms that must also have been present on the surface were not observed in these experiments. In Fig. 1D, we assign the higher and lower protrusion to

CNMe and CNHMe, respectively. An atomically resolved STM image of CNMe and CNHMe with substrate Pt atoms shows that CNMe and CNHMe are adsorbed at on-top and bridge sites, respectively (fig. S1). As is generally the case in STM images, the apparent heights of the two adsorbates are a convolution of geometric and electronic factors. Density functional theory (DFT) calculations based on simple cluster models of the adsorption sites (18) indicate that the methyl carbon of CNHMe is nearer the surface by 0.1 nm than is the methyl carbon of CNMe. Because the apparent height difference is considerably smaller than the geometric height difference, CNHMe probably provides higher conductivity between the tip and the metal substrate than does CNMe.

We achieved the reverse reaction, deprotonation of CNHMe to CNMe, by injection of tunneling electrons as shown in Fig. 2, A and B. An

STM image of both CNMe and CNHMe coadsorbed on Pt(111) is shown in Fig. 2A. The STM tip was precisely positioned over the center of a single CNHMe molecule as indicated by the arrow in Fig. 2A, and a voltage pulse (3.0 V at 1.5 nA for 1 s) was then applied with the feedback loop turned off. A rescans of the same area after electron injection (Fig. 2B) revealed that the product of the voltage pulse (P1) had the same appearance as that of CNMe.

Confirmation that P1 in Fig. 2B is in fact CNMe is provided by the STM-IETS results in Fig. 2D, which compares spectra of CNMe, CNHMe, and P1 on Pt(111). The details of how IETS measurements are performed with our instrument were reported elsewhere (8). A background spectrum taken over the bare Pt surface has been subtracted from each of the spectra shown in Fig. 2D. The CNMe spectrum indicated by the black curve in Fig. 2D exhibits

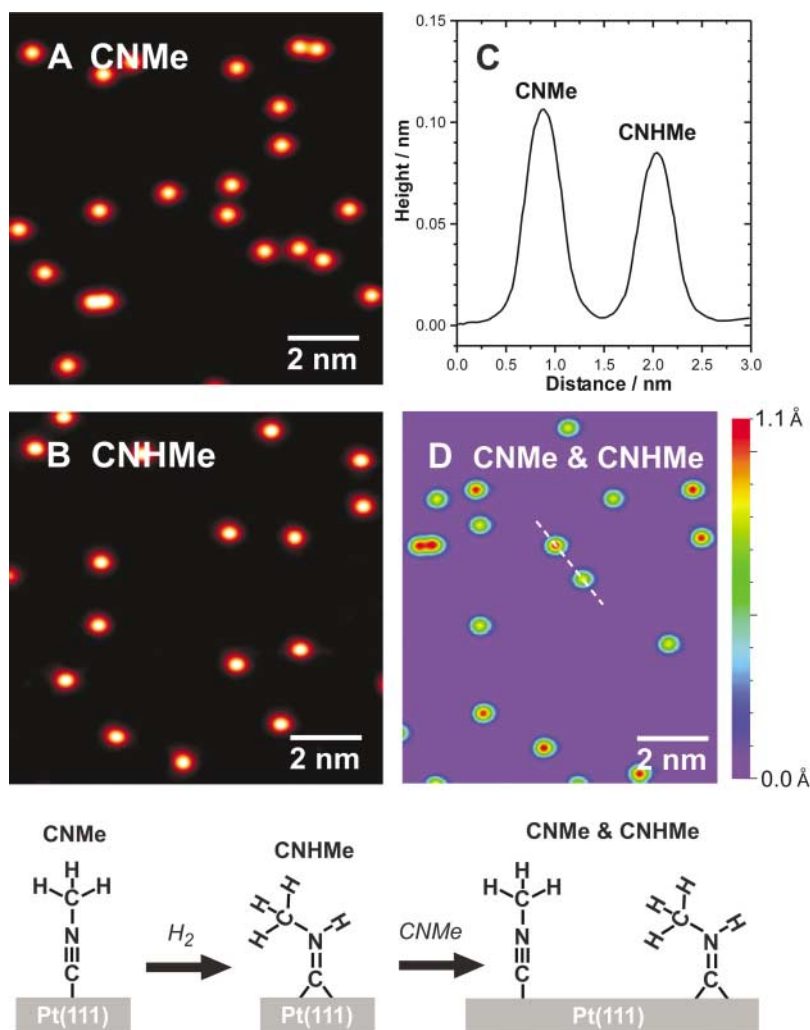


**Fig. 1.** (A) STM image of CNMe adsorbed on Pt(111). (B) STM image of CNHMe on Pt(111) obtained after exposure of the CNMe/Pt(111) surface to hydrogen ( $\text{H}_2$ ) at 300 K. CNMe and CNHMe are resolved as protrusions, and the difference in the apparent heights ( $h$ ) as shown in (C) ( $h_{\text{CNMe}} = 0.106$  nm and  $h_{\text{CNHMe}} = 0.085$  nm) is confirmed by an image obtained when CNMe was added to the CNHMe/Pt(111) surface (D). The line profile shown in (C) is taken from the dashed line indicated in (D). A schematic of the molecular species present in (A), (B), and (D) is shown at the bottom.

peaks at 8 and 48 mV for both positive and negative bias. The peak at 48 mV is readily assigned to the Pt-CNMe stretching mode, according to the high-resolution electron energy-loss spectroscopy (HREELS) study of Avery and Matheson (10). The peak at 8 meV is at too low a value to be observed with HREELS but is probably caused by a frustrated translational mode corresponding to motion of the whole molecule parallel to the surface. Assignment of a peak at 4 meV to a similar frustrated translational mode was proposed in an IETS study of benzene on an Ag(110) surface (19).

Similarly, the CNHMe spectrum (red curve) in Fig. 2D shows peaks at 9 and 34 mV at both positive and negative bias that are assigned to the frustrated translation and CNHMe-Pt

stretch modes, respectively. For the P1 spectrum (green curve) in Fig. 2D, the similarities with the CNMe spectrum allow us to definitively identify P1 as CNMe. The probability of CNHMe deprotonation to CNMe for a pulse of a given voltage for a tunneling current of 1 nA and a duration of 1 s can be obtained by dividing the number of CNMe molecules produced by the pulse by the total number of CNHMe molecules to which the pulse was applied. The voltage dependence of these probabilities is represented by the open red squares in Fig. 3A. A clear threshold at 2.8 V is evident for the CNHMe deprotonation reaction.

Further decomposition occurred when pulses of higher voltage were used. The three arrows in Fig. 2B identify CNHMe, CNMe, and P1 mole-

cules that were subjected to a 4.0-V, 2.0-nA, 1-s pulse. A single and identical product from each starting molecule was obtained and is labeled P2 in Fig. 2C. The bias dependence of the decomposition probability for CNHMe (green open triangles in Fig. 3A) shows a reaction threshold at 3.0 V, accompanied by a simultaneous decrease in the probability of CNMe formation. The voltage dependence of the P2 formation probability from CNMe almost coincides with that from CNHMe (fig. S2), indicating that decomposition proceeds via CNMe. The exact identity of P2 is not known but may be the same intermediate that occurs in the thermal decomposition of CNMe on Pt(111) (13), which proceeds with the loss of hydrogen as indicated by thermal desorption. Thus, it is reasonable to con-

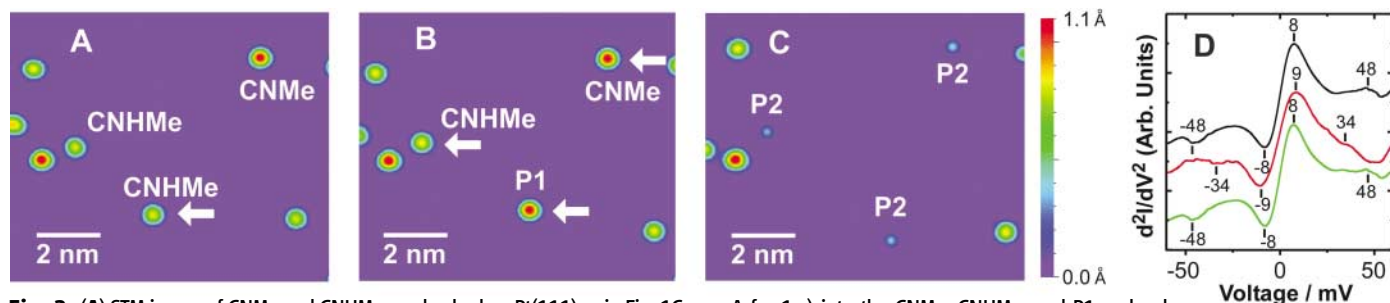


**Fig. 2.** (A) STM image of CNMe and CNHMe coadsorbed on Pt(111) as in Fig. 1C. (B) STM image obtained after the injection of tunneling electrons from the STM tip (3.0 V at 1.5 nA for 1 s) into the CNHMe molecule identified by the arrow in (A). The apparent height of the product is the same as that of CNMe. (C) STM image obtained after the injection of tunneling electrons from the STM tip (4.0 V at 2.0

nA for 1 s) into the CNMe, CNHMe, and P1 molecules identified by the arrows in (B). (D) STM-IETS spectra, in the form of the second derivative of the current with respect to voltage ( $d^2I/dV^2$ ) versus voltage, of CNMe (black line), CNHMe (red line), and P1 (green line) shown in (B). The spectrum of the Pt metal was subtracted from each spectrum shown. Arb., arbitrary.

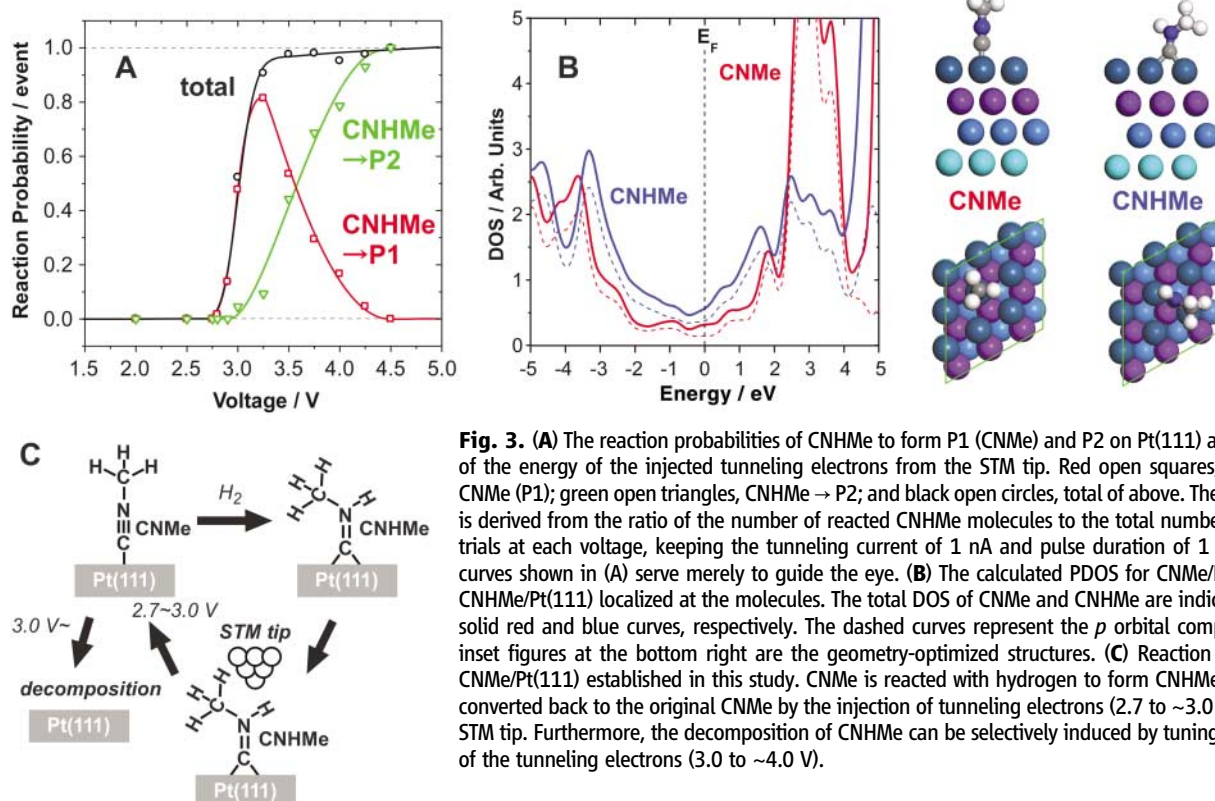


**Fig. 3.** (A) The reaction probabilities of CNHMe to form P1 (CNMe) and P2 on Pt(111) as a function of the energy of the injected tunneling electrons from the STM tip. Red open squares, CNHMe  $\rightarrow$  CNMe (P1); green open triangles, CNHMe  $\rightarrow$  P2; and black open circles, total of above. The probability is derived from the ratio of the number of reacted CNHMe molecules to the total number ( $\sim 100$ ) of trials at each voltage, keeping the tunneling current of 1 nA and pulse duration of 1 s fixed. The curves shown in (A) serve merely to guide the eye. (B) The calculated PDOS for CNMe/Pt(111) and CNHMe/Pt(111) localized at the molecules. The total DOS of CNMe and CNHMe are indicated by the solid red and blue curves, respectively. The dashed curves represent the  $p$  orbital component. The inset figures at the bottom right are the geometry-optimized structures. (C) Reaction scheme for CNMe/Pt(111) established in this study. CNMe is reacted with hydrogen to form CNHMe. CNHMe is converted back to the original CNMe by the injection of tunneling electrons (2.7 to  $\sim 3.0$  V) from the STM tip. Furthermore, the decomposition of CNHMe can be selectively induced by tuning the energy of the tunneling electrons (3.0 to  $\sim 4.0$  V).

clude that the formation of P2 involves the breaking of one or more of the C-H bonds. Furthermore, we assume that P2 is not formed by the breaking of the N-CH<sub>3</sub> bond, because the CN and CH<sub>3</sub> products of such a reaction would be readily observed as distinctly different species in the STM images.

To gain insight into the electronic states involved in these electron-induced reactions, we performed DFT calculations for CNMe and CNHMe on Pt(111) (20). The calculated partial density of states (PDOS) localized on CNMe and CNHMe is shown in Fig. 3B. The solid curves represent the total DOS of the two molecules. For both cases, the unoccupied state near the Fermi level ( $E_F$ ) mainly consists of *p*-orbital components (indicated by the dashed curves in Fig. 3B), which are mostly localized on the NC multiple bond. This result indicates that the DOS just above  $E_F$  corresponds to the  $\pi^*$  orbital, which is the LUMO (lowest unoccupied molecular orbital) for both CNMe and CNHMe. As expected, the broadening and downward shift of the  $\pi^*$  orbital that accompanies the conversion of CNMe to CNHMe are appreciable and are a manifestation of a large orbital rehybridization.

The deprotonation of CNHMe occurs selectively at the N-H bond without affecting the C-H bonds. The deprotonation threshold was observed at 2.8 V, corresponding to the LUMO ( $\pi^*$  orbital). Sainoo *et al.* reported that the interaction between chemical bonds and incident tunneling electrons is governed by the spatial distribution of the molecular orbital at the resonant level (21). Thus, the reaction efficiency should be ruled by the degree of localization of the  $\pi^*$  orbital on each H atom. The selectivity we observed is supported by calculations showing (fig. S3) that the  $\pi^*$  orbital has a greater probability density at the N-H bond than at a C-H bond. As a consequence, the broadening and downward shift of the  $\pi^*$  orbital enables the

incident electron to have a higher efficiency to enter the  $\pi^*$  orbital at lower energy. This would explain the lower threshold energy, as well as higher reaction efficiency, that are observed in CNHMe dehydrogenation.

Our findings suggest that the difficult problem of reversibility in bond-breaking reactions of single molecules can be overcome by taking advantage of the surface chemistry that naturally occurs on catalytically active metals such as Pt. The cyclic reaction scheme for the CNMe/Pt(111) system established here is summarized in Fig. 3C. CNMe reacts with hydrogen to form CNHMe through exposure to H<sub>2</sub> (gas). CNHMe is then converted back to the original CNMe through application of a voltage pulse (2.7 to ~3.0 V) from the STM tip. This cycle can be repeated to interconvert single molecules of two species with substantially different electronic and geometric structures. Alternatively, application of a voltage pulse leads to further decomposition involving the breaking of the C-H bonds of CNMe. This system thus features both bond selectivity and reversibility and thereby demonstrates an unusually high degree of control of chemistry at the single-molecule level.

#### References and Notes

1. W. Ho, *J. Chem. Phys.* **117**, 11033 (2002).
2. T. Komeda, *Prog. Surf. Sci.* **78**, 41 (2005).
3. N. Lorente, R. Ruruli, H. Tang, *J. Phys. Condens. Mater.* **17**, S1049 (2005).
4. F. Moresco, *Phys. Rep.* **399**, 175 (2004).
5. J. K. Gimzewski, C. Joachim, *Science* **283**, 1683 (1999).
6. B. C. Stipe, M. A. Rezaei, W. Ho, *Science* **280**, 1732 (1998).
7. J. Gaudioso, H. J. Lee, W. Ho, *J. Am. Chem. Soc.* **121**, 8479 (1999).
8. Y. Kim, T. Komeda, M. Kawai, *Phys. Rev. Lett.* **89**, 126104 (2002).
9. H. Ueba, *Surf. Rev. Lett.* **10**, 771 (2003).
10. N. R. Avery, T. W. Matheson, *Surf. Sci.* **143**, 110 (1984).
11. E. Schweizer *et al.*, *Surf. Sci.* **213**, 49 (1989).
12. D. H. Kang, M. Trenary, *J. Am. Chem. Soc.* **123**, 8432 (2001).

13. D. H. Kang, M. Trenary, *J. Phys. Chem. B* **106**, 5710 (2002).
14. S. Katano *et al.*, *J. Phys. Chem. B* **110**, 20344 (2006).
15. J. M. Seminario, C. E. De la Cruz, P. A. Derosa, *J. Am. Chem. Soc.* **123**, 5616 (2001).
16. J. Chen *et al.*, *Chem. Phys. Lett.* **313**, 741 (1999).
17. J. Casanova, R. Schuster, N. J. Werner, *J. Chem. Soc.* **1963**, 4280 (1963).
18. B. Chatterjee, D. H. Kang, E. Herceg, M. Trenary, *J. Chem. Phys.* **119**, 10930 (2003).
19. J. I. Pascual *et al.*, *Phys. Rev. Lett.* **86**, 1050 (2001).
20. DFT calculations were performed with the program package DMol<sup>3</sup> in Material Studio (Version 3.1) of Accelrys Inc. using the RIKEN Super Combined Cluster system. The physical wave functions are expanded in terms of numerical basis sets in the DMol<sup>3</sup> method. The double-numeric quality basis set with polarization function was used in the calculation. The generalized gradient approximation functional developed by Hammer, Hansen, and Nørskov (revised Perdew, Burke, and Enzerhof functional) was used. A Fermi smearing of 0.005 hartree (1 hartree = 27.2114 eV) and a real-space cutoff of 3.5 Å were used to improve computational performance. All electron scalar relativistic calculations were performed. Periodic 3 × 3 surface slabs, four layers thick, sampled by (2 × 2 × 1) *k* points, with a 20 Å vacuum region between the slabs, were used. The adsorbate and the two top layers of metal were allowed to relax in all of the geometry optimization calculations.
21. Y. Sainoo *et al.*, *Phys. Rev. Lett.* **95**, 246102 (2005).
22. We are indebted to M. Tamura for help with the CNMe synthesis. The present work was supported, in part, by the Grant-in-Aid for Scientific Research on Priority Areas "Electron transport through a linked molecule in nano-scale" (no. 17069006) and for Young Scientists B (grant no. 16750022) from the Ministry of Education, Culture, Sports, Science and Technology and International Joint Research Grant "Molecular wire" project (03BR1) from the New Energy Development Organization of Japan and CREST, JST. M.T. acknowledges support from the U.S. NSF under grant CHE-0135561 and from the RIKEN Eminent Visiting Scientist program.

#### Supporting Online Material

www.sciencemag.org/cgi/content/full/316/5833/1883/DC1  
Figs. S1 to S3

16 February 2007; accepted 27 April 2007  
10.1126/science.1141410

## Engineering Complex Dynamical Structures: Sequential Patterns and Desynchronization

István Z. Kiss,<sup>1</sup> Craig G. Rusin,<sup>1</sup> Hiroshi Kori,<sup>2</sup> John L. Hudson<sup>1\*</sup>

We used phase models to describe and tune complex dynamic structures to desired states; weak, nondestructive signals are used to alter interactions among nonlinear rhythmic elements. Experiments on electrochemical reactions on electrode arrays were used to demonstrate the power of mild model-engineered feedback to achieve a desired response. Applications are made to the generation of sequentially visited dynamic cluster patterns similar to reproducible sequences seen in biological systems and to the design of a nonlinear antipacemaker for the destruction of pathological synchronization of a population of interacting oscillators.

Complex system responses can emerge from interactions among nonlinear rhythmic components (1, 2). Examples abound in biology (3, 4), communications (5), population

dynamics (6), and chemical reaction systems (7, 8). Inherent feedback is often an integral component; for example, circadian rhythms are controlled by the interactions within the multi-

cellular master circadian clock in the brain, entrainment from sunlight, and feedback from other brain parts and locomotive activities (9).

External feedback can be used to control the behavior of complex rhythms, both to tune essential behavior, such as by heart pacemakers (10), or to alter pathological behavior, such as by deep-brain "antipacemakers" in tremors or Parkinson's disease (11). In such applications, a mild control is desired so that the system can be tuned to a desired behavior without destroying its fundamental nature. The efficient description and design of complex dynamic structure is a formidable task that requires simple yet accurate models, incorporating integrative experimental

<sup>1</sup>Department of Chemical Engineering, 102 Engineers' Way, University of Virginia, Charlottesville, VA 22904-4741, USA.

<sup>2</sup>Department of Mathematics, Hokkaido University, Kita 10, Nishi 8, Kita-Ku, Sapporo, Hokkaido, 060-0810, Japan.

\*To whom correspondence should be addressed. E-mail: hudson@virginia.edu